J. Phys. B: At. Mol. Opt. Phys. **29** (1996) 5475–5491. Printed in the UK

Vibrationally inelastic and elastic cross sections for $e + NF_3$ collisions

L Boesten†, Y Tachibana†, Y Nakano†, T Shinohara§, H Tanaka† and M A Dillon‡

† Department of Physics, Sophia University, Chiyoda-ku, Kioicho 7-1, Tokyo, Japan 102
‡ Argonne National Laboratory, 9700 S Cass Avenue, Argonne, IL 60439, USA

Received 26 October 1995, in final form 3 September 1996

Abstract. Absolute elastic cross sections for electron impact on nitrogen trifluoride (NF_3) have been recorded for impact energies from 1.5 to 100 eV and scattering angles from 20° to 130°. Because of the small dipole moment, estimates of the integrated and momentum-transfer cross sections were obtained by extrapolation of the angular range with the help of a modified phase-shift program and subsequent numerical integration under the fits. Vibrational excitation function measurements show a 2 eV wide resonance at 3 eV impact energy. Vibrational loss spectra were measured near this resonance and resolved into their vibrational components ν_1 and ν_3. From the angular behaviour of these fundamental modes, the resonance can be assigned to a temporary trapping of the impinging electron in the antibonding orbital of irreducible species 'e', the LUMO orbit.

1. Introduction

Nitrogen trifluoride (NF_3) belongs to the C_{3v} symmetry group. Its molecular orbitals are described in terms of the irreducible species $1a_1, 1a_2, \ldots$ and e, where the leading index distinguishes between orbitals of the same species. Similarly, the fundamental vibrational modes of NF_3 are designated as ν_1, ν_2, ν_3, and ν_4. Identical designations are used for ammonia (NH_3). Add the common illustrations of molecular vibrations for NX_3 molecules as shown in figure 1, and some serious misconceptions are bound to arise, one of which is the following.

Assume that an electron strikes one of the molecules CH_4, SiH_4, or GeH_4 of symmetry group T_d, is temporarily captured in the lowest unoccupied orbital (LUMO), and, after departure, leaves the molecule in a vibrationally excited state. Because the irreducible species of the trapping LUMOs are the same, one naturally expects an enhancement of the same vibrational mode(s) and a similar angular distribution of their differential cross sections (DCS), and indeed, such behaviour has actually been observed (CH_4: Tanaka *et al* 1983; SiH_4: Tanaka *et al* 1990; GeH_4: Dillon *et al* 1993; for a molecule of a different structure see SF_6: Randell *et al* 1992).

The order of the lowest unoccupied orbitals of both molecules is inverted (NH_3 has $4a_1$, 2e while NF_3 has 6e, $7a_1$). Also it is known that the electron trapping orbital of NH_3 is the second empty valence molecular orbital of symmetry 2e (Ben Arfa and Tronc 1988, also Gianturco 1991, p 4634). We will show below that the trapping orbital of NF_3 also

§ Present address: Anelva Co Fuchuu, Yotsuya 5-81, Tokyo, Japan 183.

0953-4075/96/225475+17$19.50

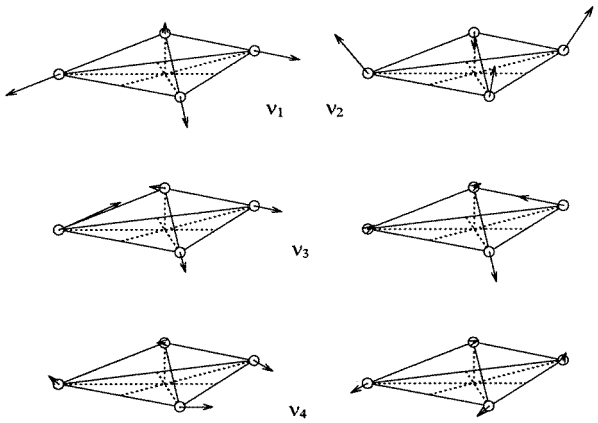

Figure 1. Fundamental modes of X_3Y molecules (after Herzberg 1945).

is 'e'. Now assume that an electron impinges on NF_3 or NH_3. The molecular structure is the same, the trapping orbitals are the same, and the enhanced vibrational modes are the same (ν_1, ν_3); however, as demonstrated in this article, the angular distributions of their vibrational DCS are different. In this particular example, we will also show that one has to be very careful with attempts to extract information about 'vibrational stretching modes' (ν_s) from the unresolved peak ν_1/ν_3. Naturally, we will continuously refer to NH_3 for comparisons.

While there have been some recent experimental measurements of low-energy electron–NH_3 collisions (elastic and vibrational DCS: Alle *et al* 1992, Ben Arfa and Tronc 1985, 1988, Gulley *et al* 1992; total cross sections: Szmytkowski *et al* 1989, Sueoka *et al* 1987) and a few theoretical studies (Gianturco 1991, Pritchard *et al* 1989), no equivalent studies exist for NF_3. The few collisional studies are entirely restricted to optical emission by electron impact (Blanks and Becker 1987, Blanks *et al* 1987, 1989, Jabbour *et al* 1988, Roque *et al* 1991), ionization (Tarnovsky *et al* 1994, Rogers *et al* 1990, Baumgärtel *et al* 1989), and dissociation and dissociative attachment (Harland and Franklin 1974, O'Keeffe 1986, Thynne 1969, Chantry 1978, Trainor and Jacob 1979, Sides and Tiernan 1977, Lakdawala and Moruzzi 1980); or they are application studies of plasmas containing admixtures of NF_3 (e.g. Donnelly *et al* 1984, Greenberg and Verdeyen 1985, Hargis and Greenberg 1990). The *Gmelin Handbook of Inorganic Chemistry* (Jäger *et al* 1986) has a good resumé of physical properties up to 1986. Quite recently, a close coupling calculation has been published (Rescigno 1995a, b) which presents a three-dimensional plot of the elastic DCS over the impact energy range from 0.2 to 10 eV and from 5° to 180° together with a graph of the momentum-transfer cross section. Unfortunately, the overlap with the range of our experiments (1.5–100 eV, 20–130°) is rather restricted.

2. Equipment and procedures

2.1. Apparatus

The cross sections were recorded at a temperature of about 330 K in a crossed-beam experiment at background pressures of 10^{-6} Torr with the gas beam turned on. Near-monochromatic electrons are produced with a computer-driven lens system following a

single hemispheric monochromator of 42 mm radius. The scattered electrons are re-accelerated in a zoom-lens system and analysed for energy loss in a second hemispheric analyser (for details see Tanaka *et al* 1990, Takagi *et al* 1994). Overall energy resolution was 35 meV (FWHM) as read off the elastic peaks recorded. Impact energies varied from 1.5 to 100 eV. The angular range from -20° to $+130^\circ$ has an estimated resolution of 2–3°. At the present energy resolution, the elastic and vibrational measurements include a small unresolved rotational component. All elastic and vibrational DCS were calibrated against a set of standard He cross sections (Boesten and Tanaka 1992) by repeating the measurements point by point with He under identical experimental conditions. This calibration requires constant Knudsen numbers for equal molecular densities in the collision volume (Brinkmann and Trajmar 1981, see also Nickel *et al* 1989). We used the pressure ratio in Trajmar's calibration formula (Trajmar and Register 1984) which is sufficiently accurate with our equipment, a simple tube nozzle with a length of 5 mm and a diameter of 0.3 mm (Takagi *et al* 1994). The impact energy was calibrated against the 19.367 eV resonance of He at 90°, and the ($\nu = 0 \rightarrow 1$) peak of N_2^- at an incident energy of 1.97 eV (Wong and Dubé 1978). The accuracy of the energy scale is limited by our sweep voltage sources with a minimum step of 10 mV (± 0.5 mV). The ordinate of the vibrational excitation functions was adjusted by comparison with the corresponding loss measurements because direct normalization from the He measurements produced too much scatter. In these measurements the control of the input electron beam is less than ideal.

We use a very detailed electron-tracing program with automatic focus-finding routines that allow several conditions like position, beam diameter, beam angle etc to be imposed (Boesten 1988) and have worked out a set of driving voltages for all lenses, including the entrance lens of the detection system. They maintain a stable virtual aperture at the entrance of the energy selector over the full range of electron energies (= residual energies), except for the pencil angle that follows the Helmholtz–Lagrange law (Kuyatt and Simpson 1967) and the beam angle that we restrict to less than 5.7°. The passing energy of the selector and all following voltages remain constant. Thus we expect a flat response of the analyser throughout the *whole* energy range. We have verified its performance as follows. When measuring the elastic differential cross sections of a gas we always monitor the elastic DCS of He as counts/(sweep $\times$ backing pressure) and plot their angular behaviour as a check against poor electron-beam adjustments. These counts can be also interpreted as an attempt to measure the He DCS directly and thus should reflect their theoretical values. The ratio of the normalized counts to the theoretical He DCS (at 90°, multiplied by 5.61) was 0.998 ± 0.16 over the full range† of residual energies from 1.5 to 100 eV. The deviations are randomly distributed and their position varies from gas to gas. Large systematic variations of the analyser response function as reported by Nickel *et al* (1989; variation 1:5.5) are thus excluded. The deviations arise from the manual adjustments of the *impact* electron beam; the operator was not aware of the connection to the theoretical DCS. Note that the calibration formula from above automatically eliminates these deviations.

2.2. Extrapolation and integration

The elastic cross sections were extrapolated to 0° and 180° with the help of modified phase-shift fitting that uses the Thompson correction for higher phases (Thompson 1966), an overall size parameter (Register *et al* 1980), and incorporates inelastic phase-shift fitting (Bransden 1970) above 15 eV as described recently (Takagi *et al* 1994). The polarizability

† Maximum deviations were ± 0.27. We have removed one obvious outlier (1.55) at 5 eV from the series: 2.26, 2.66, *1.55*, 2.57, 2.51 of nearby counts. Its ratio would be 1.50.

was set at 3.26×10^{-24} cm^3 (Weast 1987). The sole purpose of these extrapolations is to obtain the integrated (Q_I) and momentum transfer (Q_M) cross sections needed in plasma modelling. Note that these integrals are fairly insensitive to details of the extrapolation tails due to the $\sin\theta$ factor in the integration formulae,

$$Q_I = 2\pi \int \mathrm{DCS}(\theta) \sin\theta \, \mathrm{d}\theta \tag{1}$$

$$Q_M = 2\pi \int \mathrm{DCS}(\theta)(1 - \cos\theta) \sin\theta \, \mathrm{d}\theta. \tag{2}$$

In view of the strong warning against the extrapolating experimental cross sections of water (Okamoto *et al* 1993) we inquired with the authors of that paper (Onda 1994) about NF_3. Quoting the very different dipole moments (H_2O: 0.728 au, NH_3: 0.578, NF_3: 0.0944) they pointed out that the dipole interaction between the electron and NF_3 would not be important in this collision system. The point–dipole cross section q^B in the Born approximation—which gives a fairly good approximation for angles $\theta \leqslant 10^\circ$—scales with the square of the dipole moment (Okamoto *et al* 1993).

At higher impact energies, our fits develop many local minima among which one has to choose by selecting a different L at which the Thompson correction sets in, or different initial values for phase-shifts and the size factor. Fits that develop a *deep* minimum at around 150° in a log(DCS) plot, or that rise very steeply towards 180° are rejected. Some fits produce values of Q_I which connect into a smooth curve of $Q_I(E_{impact})$, but form a ragged trace for $Q_M(E_{impact})$ or vice versa; they are rejected. We accept only fits that converge fully without artificial interruption, converge reasonably fast, have a low χ^2 criterion, and fulfil all the above and other shape-related criteria, all simultaneously. We have no objection if the reader wishes to classify these fits as an elaborate way of drawing manual extrapolations, but in the past they have approximated theory rather closely (e.g. Boesten and Tanaka 1991). The fits are included in figure 2, but should not be interpreted as our estimate for the low and high angle DCS.

2.3. Peak 'unfolding'

Under this term we understand resolving a compound peak like ν_1/ν_3 into its components ν_1 and ν_3, a process which can also be applied to overtones or combination frequencies. After subtracting the background signal established in a separate recording, we derive the apparatus function from the elastic line shape with some minor manual corrections in the tails ($\approx 1\%$ of the peak value). We assume the same shape to be present at all fundamental, overtone, and combination frequencies included in the analysis and determine the height of these peaks by a least square fit in such a way that the sum of the peaks approaches the observed spectrum as close as possible. All peaks are fitted simultaneously. This procedure is linear in the coefficients and thus unique as are least square polynomial fittings. The only arbitrariness arises from the selection of the frequencies to be included. Hardly any alternative choices exist at low energy losses, and the peak unfolding becomes unique. Details of this procedure, its statistical capabilities and limits are discussed in the appendix.

3. Results

3.1. Elastic differential cross sections and their integrals

The normalized elastic cross sections are shown in figure 2 and are listed in table 1, together with their integrals. For comparison, we add a similar plot for NH_3 (Alle *et al* 1992). Error

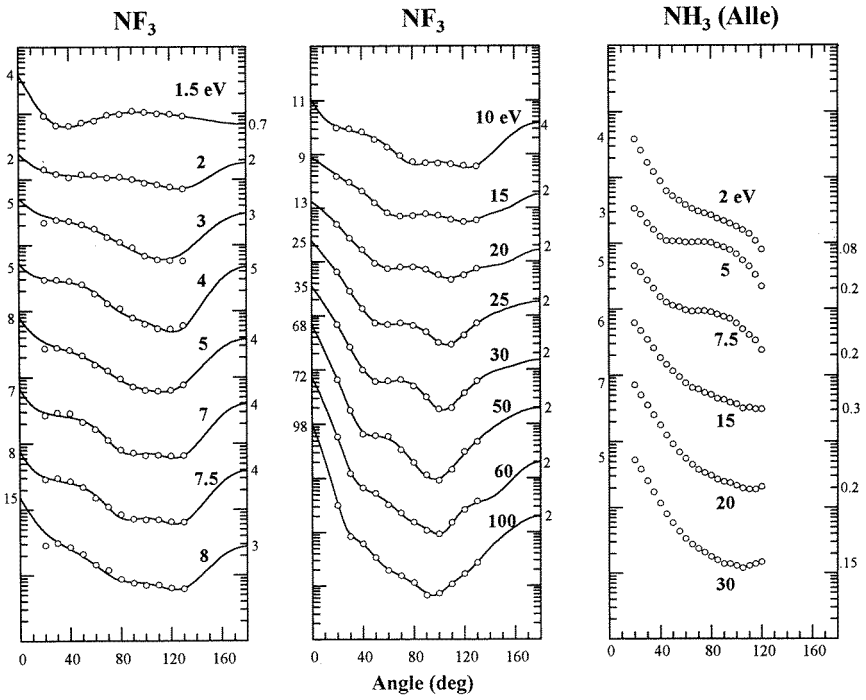

Figure 2. Elastic DCS of NF_3 and NH_3 (Alle *et al* 1992). The full curves show our extrapolations. The ordinate labels give the approximate value of the closest point on the nearby curve.

estimates are as follows: the He reference data are accurate to about 10%, the elastic DCS counts introduce another 10% statistical error, giving a total of about 15%.

Some physical properties of these two molecules are collected in tables 2 and 3. The nomenclature $\nu_1, \nu_2, \nu_3, \nu_4$ has been consistent since Herzberg (1945), Shimanouchi (1972) and up to the present time (Jäger *et al* 1986); some authors prefer to call ν_2 'umbrella mode'. In scattering from central potentials the dominant partial cross sections σ_ℓ shift towards higher ℓ with an increase in the effective radius of the potential (Landau and Lifshitz 1965, section 123), and the number of minima in the elastic cross sections as a function of scattering angle increases (Schmid *et al* 1988, Koonin 1986). It is thus tempting to attribute the 'bumpy' shape of NF_3 (i.e. the appearance of higher ℓ-components) to the larger size of this molecule; however, Itikawa and Nishimura (1995) have pointed out that such a structure may rather be connected with the number of electrons (also see Johnstone and Newell 1993). The angular distributions of isoelectronic scatterers are usually quite similar.

The flat distribution of NF_3 at low incident energies when compared with the steep descent of NH_3 is unexpected, however (see figure 2). A similar dip has been found in N_2O, another polar molecule with a small permanent dipole moment ($0.167D$; see Johnstone and Newell 1993). Certainly, the large molecular dipole moment of NH_3 favours forward scattering but, according to theory, does so at *all* impact energies with some peaking at 20 eV, the maximum energy of Gianturco's (1991) calculation. Thus, it is unlikely that the dipole moment of NF_3 can explain the differences at low energies. Experience with other polar molecules (CO: Onda and Truhlar 1980; H_2O: Okamoto *et al* 1993 versus Johnstone

Table 1. Elastic DCS in Å^2 sr^{-1} and their integrals[a] Q_I and Q_M in Å^2.

Angle	1.5 eV	2 eV	3 eV	4 eV	5 eV	7 eV	7.5 eV	8 eV
20	0.933	1.430	2.199	2.960	2.729	2.671	2.896	2.908
30	0.667	1.216	2.436	2.949	2.807	2.932	3.036	3.132
40	0.656	1.078	2.331	2.822	2.577	2.868	2.731	2.699
50	0.729	1.197	2.052	2.511	2.119	2.123	2.224	2.115
60	0.787	1.152	1.768	1.818	1.552	1.655	1.517	1.460
70	0.962	1.074	1.329	1.297	1.261	1.137	1.108	1.209
80	0.981	1.100	1.114	1.099	0.947	0.808	0.851	0.868
90	1.097	1.011	0.920	0.794	0.714	0.727	0.719	0.766
100	1.053	0.884	0.685	0.640	0.641	0.663	0.704	0.702
110	0.998	0.843	0.598	0.542	0.622	0.666	0.704	0.707
120	0.992	0.778	0.584	0.539	0.637	0.652	0.661	0.639
130	0.920	0.723	0.576	0.604	0.765	0.655	0.645	0.623
Q_I	11.90	12.98	17.24	18.41	18.11	17.35	17.47	17.89
L%	4	5	7	7	8	7	8	13
R%	15	18	19	20	21	20	20	15
Q_M	12.46	12.39	14.24	14.92	14.92	14.24	14.17	12.82
R%	28	31	44	47	48	47	46	41

Angle	10 eV	15 eV	20 eV	25 eV	30 eV	50 eV	60 eV	100 eV
15	3.323	4.641	6.890	9.051	10.710	12.330	11.200	9.000
20	3.168	3.946	5.006	6.490	6.946	6.715	5.955	3.201
30	3.037	3.077	2.777	2.863	2.657	1.838	1.243	0.851
40	2.680	2.107	1.680	1.358	1.004	0.666	0.671	0.623
50	1.934	1.271	0.934	0.742	0.616	0.621	0.537	0.340
60	1.390	0.826	0.750	0.688	0.639	0.601	0.328	0.195
70	0.954	0.715	0.799	0.747	0.671	0.340	0.232	0.156
80	0.737	0.725	0.798	0.665	0.509	0.196	0.155	0.116
90	0.702	0.786	0.715	0.510	0.320	0.116	0.109	0.067
100	0.694	0.738	0.569	0.322	0.191	0.093	0.093	0.073
110	0.673	0.610	0.462	0.295	0.200	0.146	0.152	0.108
120	0.626	0.555	0.561	0.440	0.376	0.314	0.265	0.169
130	0.605	0.598	0.746	0.725	0.623	0.483	0.378	0.273
Q_I	16.91	14.60	14.48	14.05	13.33	12.32	11.03	9.72
L%	6	9	13	18	24	35	41	47
R%	20	14	14	17	15	62	13	17
Q_M	13.53	10.41	9.87	8.54	7.63	6.62	5.81	5.42
R%	47	37	39	50	52	63	58	70

[a] Q_I is the integrated elastic cross section, Q_M the moment transfer cross section; L% and R% are the contributions of the low and high angle extrapolations in per cent. L% of Q_M is smaller than 1.3% for all impact energies.

and Newell 1991; O_3, N_2O, H_2S, and SO_2: Buckman *et al* 1994) seems to indicate that dipole-enhanced forward scattering is restricted to small angles, usually below 10–20°. This has been confirmed again in the recent calculations of Rescigno (1995b) whose DCS at 20° reflect our data. The small molecular dipole moment of NF_3 itself is due to the electronegativity of the fluorine atoms pulling in the bonding electrons (Jäger *et al* 1986, pp 184ff, Bawagan and Brion 1987, 1988).

Table 2. Constants[a] for NF_3 and NH_3.

	NH_3	NF_3
Atomic radius of F or H (Å)	0.373	0.709[a]
Bond length (Å)	1.012	1.365
XNX angle	106.7°	102.4°
Vertical first ionization potential (eV)	10.16	13.0
Dipole moment (D)	1.468	0.235

[a] Bond and angles (II, pp 654–60), ionization (II, p 579), and dipole moment (II, p 720) are from Nihon-Kagakkai (1984). Atomic radii are from Fluck and Heumann (1991). Gillespie and Robinson (1992) propose a covalent radius of 0.54 Å for the fluorine. Electron-impact ionization of NF_3 occurs at 13.5 eV (Tarnovsky *et al* 1994).

Table 3. Vibrational frequencies in eV.

Frequencies	Designation		NH_3	NF_3
a_1 ν_1	symmetric stretch	0.4138[b]	0.4768[c]	0.1280[d]
a_1 ν_2	symmetric bend/deformation[a]	0.1178	0.1267	0.0802
e ν_3	asymmetric/degenerate stretch	0.4271	0.4490	0.1125
e ν_4	asymmetric bend	0.2017	0.1678	0.0611

[a] Also called 'umbrella mode'.
[b] Shimanouchi (1972, p 15), Herzberg II p 295 (1945, but $\nu_3 = 0.4233$).
[c] Experimental values listed in Thomas *et al* (1993).
[d] Jäger *et al* (1986, p 192), Shimanouchi (1972, p 16).

Three-dimensional plots of the two sets of elastic DCS are shown in figure 3(*a*) for the full angular and energy ranges of table 1 except 5 eV. The smooth 'waves' of NH_3 contrast strongly with the many 'bumps' in NF_3. An as yet unexplained 'valley' or ridge extends from the high peak of the NF_3 traces (100 eV, 20° corner) diagonally down toward the viewer (1.5 eV, 130° corner). This structure becomes much clearer on rotating the (100 eV, 130°) corner to the front, see figure 3(*b*) where we have added a similar plot for C_2F_6 (Takagi *et al* 1994). So far, we have found such a structure in all scattering experiments where the H of hydrocarbons has been replaced by F (CF_4, C_2F_6, C_3F_8, and a very faint trace in CH_2F_2), and also in other F-containing molecules (NF_3 and SF_6); and we wonder whether we are seeing a common feature of the fluorine. Replacing C with the heavy Si or Ge while retaining H does not produce this feature, and so size alone is insufficient as an explanation.

Integrated elastic DCS, Q_I, and momentum-transfer cross sections, Q_M, are shown in figure 4 and listed at the bottom of table 1. We presume that the error from the extrapolations amounts to 30–50% of their contributions; they are not *entirely* unreasonable. The contributions are indicated in table 1. While the sagging of Q_M on the high energy side may be due to imperfections of the fits, the crossing at 1.5 eV arises from the observed DCS themselves. Here it would be difficult to lower Q_M much further than the present fit. The crossing reflects the flat shape of the elastic DCS at low energies. Rescigno's (1995b) momentum-transfer cross sections peak at the correct energy with the correct size but are narrower, a well known trend in such calculations (Huo 1995). No comparable experimental data are available in the literature. We have included a rough sketch of the integral cross sections of NH_3 for which data are scanty. The broad peak at around 4–5 eV in NF_3, somewhat shifted from that of vibrational excitation (3 eV; see figure 4), finds its

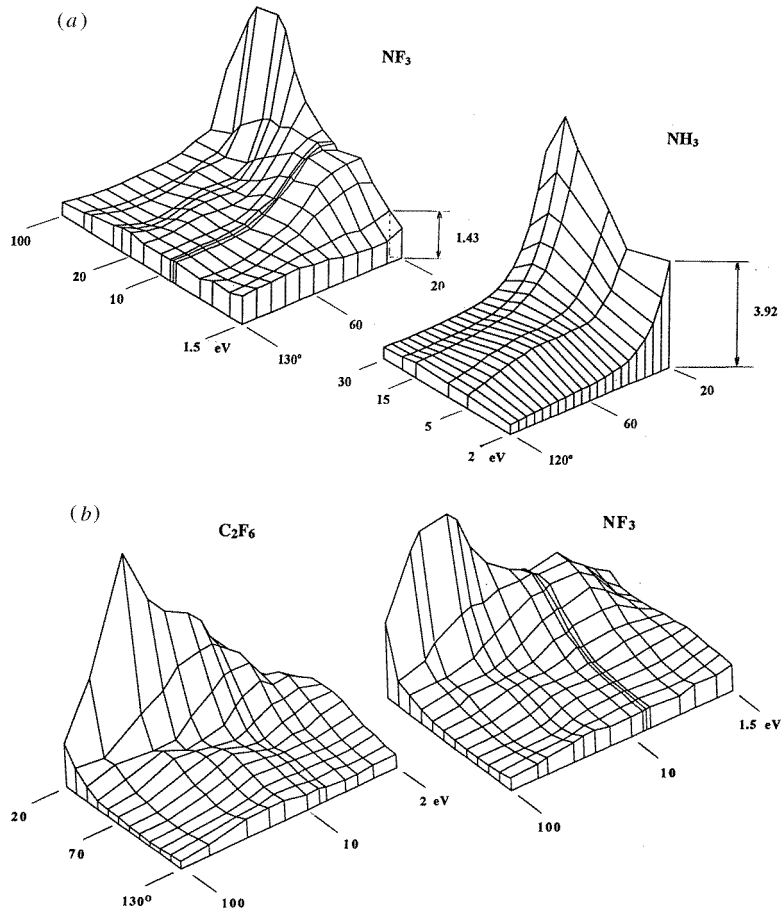

Figure 3. (*a*) Three-dimensional plots of the DCS of NF_3 and NH_3. The vertical scale of both plots is linear and approximately equal. (*b*) The same plot of NF_3 rotated to bring out the ridge/valley mentioned in the text, together with a similar plot of C_2F_6.

parallel in NH_3 with a similar shift: $Q_I = 9$ eV (Alle *et al* 1992), $Q_{vib} = 7.4$ eV (Ben Arfa and Tronc 1985).

Quantum Mechanics by Landau and Lifshitz (1965, section 132) contains a simple exposition of resonances from quasi-discrete levels that shows that the phase of the outgoing electron changes by π when going through the resonance region. Thus it is only natural that theoreticians inspect eigenphase sums to obtain information on resonances. An excellent example can be found in Gianturco and Thompson (1980). They obtain a phase change of 0.8π for H_2S over an interval as short as 0.5 eV and try to connect it with an experimentally observed resonance. For NH_3, however, Gianturco (1991) finds a steady one-π rise in the eigenphase sum of the irreducible representation 'e' over a very wide energy range from 1 to 20 eV and attributes this to the existence of a temporary anion of that symmetry with a very short lifetime. But the half-widths of the vibrational excitation functions of both NH_3 and NF_3 (approximately 2 eV each) and the half-widths of Q_I of both NH_3 and NF_3 (approximately 50 eV each, with long tails) are so discrepant from Gianturco's width (20 eV) that they may be separate resonances or separate phenomena.

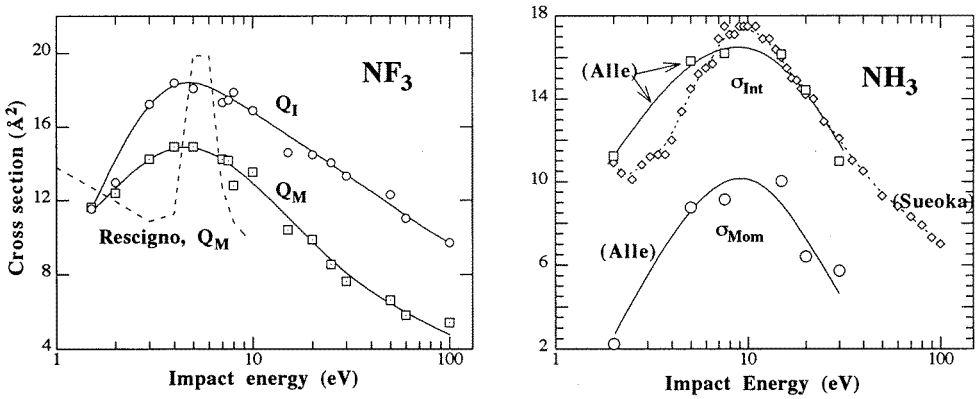

Figure 4. Integrated Q_I and momentum transfer Q_M cross sections of NF_3 obtained by extrapolation and numerical integration of the DCS of figure 1. The lines of NH_3 are intended as visual helps. Open squares: from a table in Alle *et al* (1992); open diamonds: Q_{tot} (not Q_I!) from a table in Sueoka *et al* (1987). Broken curve: Schwinger calculation of Rescigno (1995b) and private communication.

3.2. Vibrationally inelastic cross sections

Obtaining information on resonances from elastic DCS or integrated cross sections in the range of energies considered in this paper, 1.5–100 eV, is difficult. Fortunately, direct scattering in vibrational excitation (the constant term in the Breit–Wigner formula, Hall and Read (1984)) is small and the resonance may then appear as a Lorentzian peak in plots of DCS versus impact energy. When the extra electron is temporarily trapped in a potential valley created by the combination of an attractive potential and the centrifugal potential, the resonance is called a shape resonance and usually short-lived, i.e. is broad. Figure 5 shows such a shape resonance in the vibrational excitation function at the energy loss of the compound peak ν_1/ν_3, or about 0.12 eV. The 90° measurement actually extends out to 17 eV. The single peak of width of ≈ 2 eV at an impact energy of 3 eV is of a size that corresponds roughly to 10% of the elastic peak. It is angle-independent as expected of resonances.

We have recorded selective $(30°, 60°, 90°, 120°)$ loss spectra off-resonance at 1.5, 4, and 7 eV and a complete set of spectra at the resonance energy of 3 eV from 20 to 130°. A sample is shown in figure 6. This figure includes the results of 'unfolding' the compound peak ν_1/ν_3 as explained above. We use the heights of subpeaks ν_1 and ν_3 to discuss the general trend of their angular distribution (e.g. where a minimum occurs), and the *position* of their overtones up to $4\nu_1$ to distinguish between ν_1 and ν_3. Modes ν_2 and ν_4 are included only to fill the valley near 0.07 eV so that the estimate of ν_3 does not suffer. Figure 7 shows the resulting angular plots for modes ν_1, ν_3, and the compound peak ν_1/ν_3 at an impact energy of 3 eV. Obviously, the compound peak ν_1/ν_3 of NF_3 bears little resemblance to either ν_1 or ν_3. Identifying the first loss peak ν_1/ν_3 of NH_3 as mainly ν_1 was possible because harmonics were restricted to multiples of ν_1, with some admixture of $n\nu_4$ (Ben Arfa and Tronc 1985). In NF_3, the harmonics involve $n\nu_3$ and not $n\nu_1$ (see figure 6), but ν_1 is strongly present in the compound peak itself. For comparison, we have included the corresponding angular distributions of NH_3. Obviously they are of an entirely different symmetry.

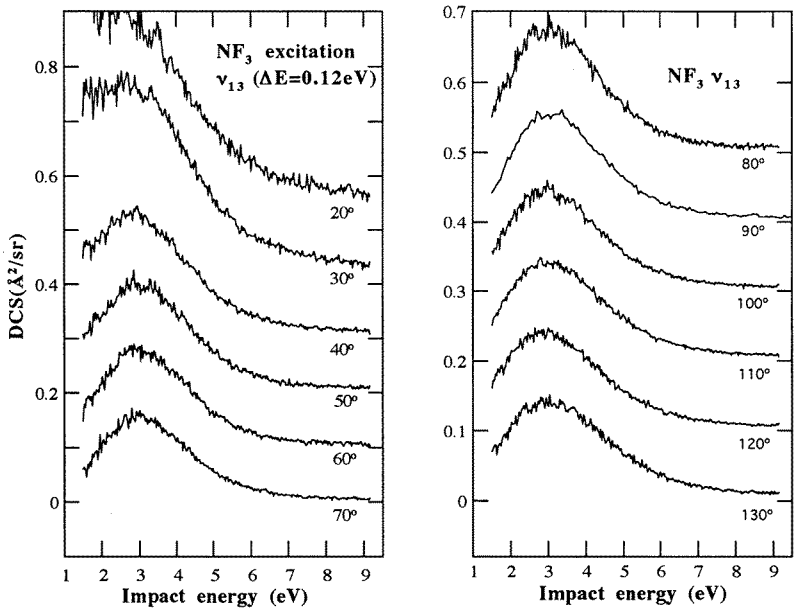

Figure 5. Excitation function for the compound peak ν_1/ν_3 at an energy loss of 0.12 eV. The traces are shifted up by 0.1 units, each, and approach zero at the right. Stray electrons from the primary beam partly obscure the relatively large peak at 30°. At 20° the peak is difficult to discern, but does exist (cf figure 7).

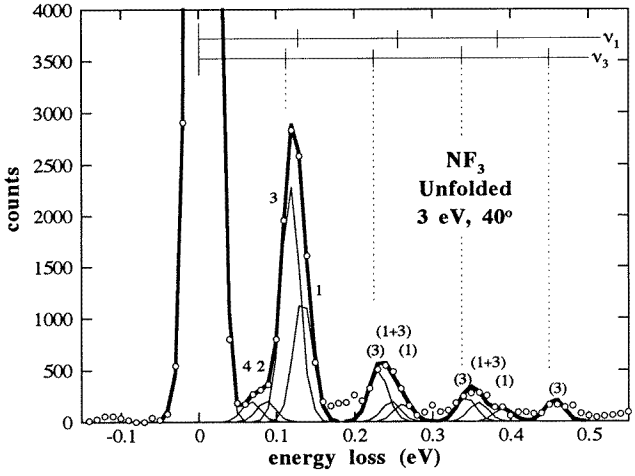

Figure 6. An electron-loss spectrum at the resonance incident energy of 3 eV (open circles) fitted with the sum of the subpeaks obtained by unfolding. Open circles: measurements; bold full curve: fitted curve; numbers: fundamental frequencies; bracketed numbers: harmonics or combination levels. There may be a small superelastic peak at −0.11 eV. To avoid confusion only subpeaks used in the analysis have been included in this plot. If the valley at 0.2 eV is properly filled up (e.g. by adding $2\nu_2$ and $3\nu_4$) the sizes of ν_1 and ν_3 change slightly (ν_1: −4%, ν_3: +2%).

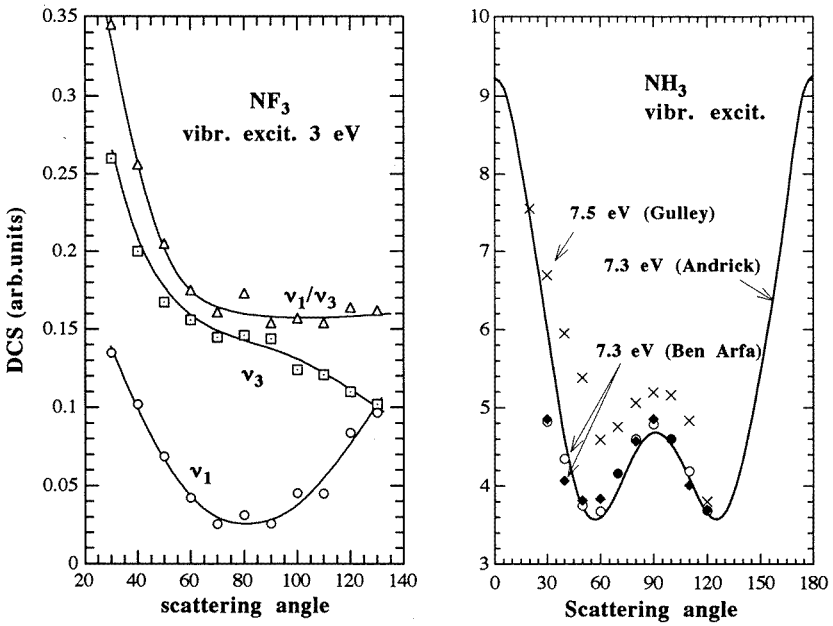

Figure 7. Angular distributions of some fundamental modes of NF_3 at the resonance impact energy of 3 eV, together with equivalent data for NH_3 (crosses: Gulley *et al* (1992); open circles: ν_1/ν_3; full diamonds: $2\nu_1/\nu_3$; both from Ben Arfa and Tronc (1988)). The compound peak ν_1/ν_3 of NH_3 mainly contains ν_1. The trace of $2(\nu_1/\nu_3)$ has been scaled up to coincide with ν_1/ν_3. The full curve (theory, Andrick and Read (1971)) is symmetrical around 90°.

4. Discussion

Further information about the resonance in the vibrational excitation has been obtained from a Gaussian 92 calculation (Frisch *et al* 1992) of the lowest unoccupied orbitals (called virtual orbitals) with minimal basis set STO-3G and subsequent symmetry analysis. Virtual orbitals are variationally not stable, and thus advanced basis sets like RHF/6-31G* or higher can obscure the true LUMO information (Chen and Gallup 1990). This observation was confirmed in a series of 15 calculations on various hydrocarbons and their fluorine equivalents and in other molecules measured in our laboratory. We have found only two exceptions to the 'rule' that the LUMO from a STO-3G calculation is the trapping orbital. One of these exceptions is NH_3; here, higher basis sets result in the same ordering of orbitals. The two lowest unoccupied orbitals are 'e' = 12.75 eV and 'a_1' = 13.24 eV for NF_3, and 'a_1' = 17.43 eV and 'e' = 19.89 eV for NH_3, where the energies are those of STO-3G. As in previous publications we include the two lowest virtual orbitals of this calculation in the following symmetry analysis and decide from the scattering observations themselves which one is the trapping orbital. We have performed a standard symmetry analysis according to angular correlation theory (Andrick and Read 1971), combined with direct product rules (Wong and Schulz 1975), and show the results in table 4 (for details, see Boesten and Tanaka 1992). Cases A1 and E arise from the inclusion of the two lowest virtual orbitals of species 'a1' and 'e' while cases E1 and E2 distinguish different possibilities of the outcome, the final vibrational state of the molecule. Unfolding at the resonance has shown the presence of both ν_1 and ν_3. Without any need to recur to ν_1, the (strong) presence of ν_3 in the compound peak and in the overtones (cf figure 6) indicates that the trapping orbital must be of symmetry

Table 4. Symmetry analysis according to point group C_{3v}.

Species	Case E1	Case E2	Case A1
Γ_{TNI}	e	e	a_1
Γ_{final}	a_1	e	a_1
ν	ν_1, ν_2	ν_3, ν_4	ν_1, ν_2
$\Gamma_{wave-out}$	e	a_1, e	a_1
ℓ_{out}	1, 2	0, 1, 2	0, 1

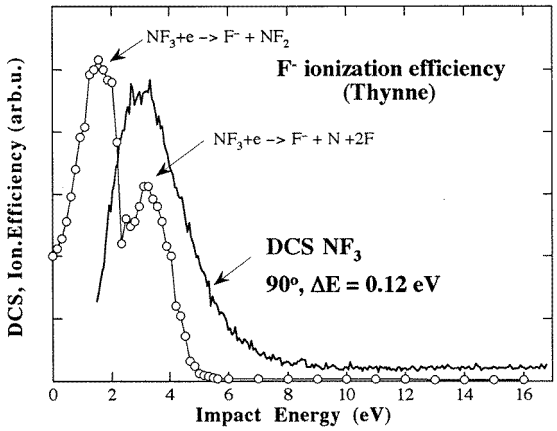

Figure 8. Vibrational excitation function of NF_3 at an energy loss of 0.12 eV and scattering angle of 90° together with various electron attachment efficiencies from Thynne (1969).

species 'e' (see row ν of table 4). A confirmation of this result is obtained as follows. The table also includes the angular moment ℓ_{out} for the outgoing electron wave in body frame coordinates. Because the angular distribution of ν_1 of figure 7 in the laboratory frame shows the behaviour of a Legendre polynomial $P_k = P_2(\theta)$, the allowed values of ℓ in the body frame can be either $\ell = 1$ or $\ell = 2$ (cf Andrick and Read 1971, equation (7)). Similarly, if the general trend of ν_3 in figure 7 is identified with $P_k = P_1(\theta)$, we obtain $\ell = 0, 1, 2$ for the scattered electron angular momentum in body-frame coordinates. In short, the observed angular distribution of the scattered wave is in accord with the symmetry analysis of table 4.

Further evidence for the temporary negative ion (TNI) at 3 eV arises from electron attachment experiments. A TNI can decay into various channels, one of which is re-emission of the electron with excitation of vibrational modes as discussed so far; another is dissociative attachment (see figure 8). Thynne (1969) derived the particular decay $NF_3 \rightarrow F^- + N + 2F$ at the impact energy of 3 eV from enthalpy considerations on his measurements. It was later confirmed by Harland and Franklin (1974) but does not seem to be a dominant process in plasma discharge (Greenberg and Verdeyen 1985). Our study gives the physical interpretation for Thynne's observation, i.e. a temporary negative ion formed by trapping the electron in the centrifugal barrier of a shape resonance associated with anti-bonding virtual orbital 'e'. Unfortunately our spectrometer does not cover the region below 1 eV reliably enough to allow similar investigations for the first peak of figure 8.

According to the Gaussian calculation the main difference between the electron-trapping

orbitals 'e' of NF_3 and NH_3 is the involvement of the p_F orbitals of NF_3 instead of the s_H orbitals of NH_3 and, of course, there are many more occupied orbitals in NF_3. An electron trapped temporarily in these orbitals changes the force balance in the molecule and thus excites vibrations. One of the degenerate 'e' orbitals is mainly concentrated along the H–N–H or F–N–F bonds. The other spreads over all four atoms in NH_3 but it is more strongly concentrated along one single N–F bond in NF_3. We presume that this asymmetry together with the vector-like nature of the p_F-atomic orbitals favours an excitation of degenerate vibration mode ν_3 without suppressing symmetrical mode ν_1 entirely. Indeed, enhancement of fundamental mode ν_3 in NF_3 is stronger than that of ν_1 if one considers size and the presence of harmonics (see figure 6) while a similar inspection of the loss spectrum of NH_3 indicates a stronger presence† of totally symmetric channel ν_1. But note that the resolution of the NH_3 experiments is lower than ours and the comparison may be biased.

5. Conclusion

Several recent studies have attempted to calculate electron scattering from a fluoro-carbon molecule (Winstead *et al* 1993, Gianturco *et al* 1994: CF_4). The attempts are encouraging but the results are not yet convincing, especially for low energy DCS. NF_3 presents yet another challenge. We hope that the present measurements provide enough detail for further theoretical investigations over a wide range of impact energies.

Acknowledgments

We wish to thank Professor K Onda of the Science University of Tokyo for consultations about the influence of the dipole moment on forward electron scattering. This work was supported by Grant in Aid from the Ministry of Education, Science, and Culture, Japan and by the US Department of Energy, Office of Energy Research, under contract no W-31-109-Eng-3.

Appendix. Statistical investigation of the unfolding procedure

Separation of overlapping peaks, or 'unfolding' (Nickel *et al* 1989, p 737L), also called 'decomposition' (Nickel, figure 4), 'resolution', 'resolving' (Gladney *et al* 1969) or 'curve-fitting' by least square methods was a topic discussed in the earlier days of electronic computing, for example under the title of 'Computer assisted gas–liquid chromatography' (Gladney *et al* 1969, Roberts *et al* 1970 and literature cited there) or 'Fitting of curves to infrared band envelopes' (Pitha and Jones 1966), albeit on less noisy data than can be expected in electron–molecule collisions. These papers discuss the feasibility of much more elaborate fitting procedures where the position of the peaks, their height, their width and skewedness (in a skewed Gaussian function approximation) become fitting parameters, i.e. nonlinear least square fitting. They point out the need for 'Intelligent implementation by the user' (Roberts *et al* 1970, p 888) and the possibility that even non-converging parameters may result in a rather close fit (Roberts *et al* 1970, p 892). Pitha and Jones (1966) give a

† The initial letter of Ben Arfa and Tronc (1985) shows a loss spectrum identified as ν_1, to which only harmonics of ν_1 fit well (our analysis). The excitation function of this mode peaks at 7.3 eV and has a half-width of 1.8 eV. In Ben Arfa and Tronc (1988) the loss spectrum is now identified as $\nu_{1,3}$, and an excitation function of $2\nu_{1,3}$ is given that peaks at 7.3 eV and has a half-width of 3 eV. Gulley *et al* (1992) confirmed the latter width for the unresolved $\nu_{1,3}$ peak but with an instrumental energy resolution of 60 meV.

successful example of 16 overlapping peaks with 65 fitting parameters for data with a noise level of 1–2% (our estimate from their plot), but also warn the reader to do a careful check of the uniqueness before any physical interpretation (p 3035).

Recent examples of peak unfolding with known peak positions are Auger electrons from krypton (Jauhiuainen *et al* 1995), electron transfer cross sections for He^+–Na collisions (Thomsen *et al* 1995) and, very close to our example, $e + CO_2$ vibrational cross sections (Johnstone *et al* 1995). An iterative decomposition of a rather noisy nitrogen energy loss spectrum into 6–7 vibrational series plus electronic state excitations was proposed by Nickel *et al* (1989).

Here we investigate a much less ambitious problem, a *linear* least square fit to the envelope of two overlapping peaks (ν_1 and ν_3) of known position, separated by 0.0155 eV or roughly half the instrumental resolution of the spectrometer in a series of numerical simulations. A possible inclusion of $2\nu_4$ at 0.1222 eV, or 0.0058 eV from ν_3 is discussed separately below.

A.1. On the unfolding of ν_1 and ν_3

The shape of the peak is derived from the elastic peak of figure 6, symmetrized slightly at the tails to give counts of 0, 110, 430, 1700, 9260, 22 800, 34 800, 22 800, ... at steps of 0.01 eV, i.e. 11 non-zero points per peak. This peak becomes the apparatus function and is placed at 0 eV to imitate the elastic peak, with scaled-down versions (7% for ν_3 and 3.5% for ν_1) at 0.1125 eV (ν_3) and 0.128 (ν_1) eV. Poisson noise would be smaller than 3% for all peaks. To be on the safe side, we superimpose a 10–30% relative white noise (details below) upon the *three* raw peaks generated. The noise-loaded peaks are then analysed by our peak-unfolding routine for the ratio of peak heights ν_3/ν_0 and ν_2/ν_0 where ν_0 indicates the (noisy) elastic peak.

Uniform deviates in the interval 0–1 with a specified standard deviation are generated from the Microsoft-provided congruential random number generator according to

$$y = y_{\text{avg}}[1 + \alpha(\text{RND} - 0.5]$$

where RND is the MS random number, y_{avg} the intended mean (in our case the raw count) and α is connected with the standard deviation of y by $\text{STD} = \alpha/\sqrt{12}$ (Korn and Korn 1968). The random number generator is seeded (randomized) anew for every repetition of the simulation. Normal (= Gaussian) deviates are generated according to the Box–Muller method from a pair of uniform random numbers (Press *et al* 1988, pp 204ff). In one further application of the MS generator we produce a random number with mean 100 as a check of the random numbers themselves. More than 10 simulations of various noise contributions, each with at least 120 repetitions, were investigated and plotted (peak height versus repetition). They show that our unfolding procedure converts an originally uniform noise distribution into an approximately normal distribution. This is to be expected since the algorithm forms a weighted average of the 11 non-zero points in the estimate of peak-height and a normal deviate can be created from the sum of 12 uniform random numbers (Abramowitz and Stegun 1972, p 953). Table A1 shows the results of three simulations. Especially note the maximum and minimum deviations, a seldom-shown statistic, since outliers of experiments are often discarded before further analysis.

The algorithm calculates the vibrational peak sizes from the ratio to the elastic peak so that two errors of standard deviation σ are involved and the combined error should be $\sqrt{2}\sigma$. We attribute the obviously better performance to the weighted averaging implied in least square fitting, also see table A2. The standard errors of the recovered peaks are close

Table A1. Simulated distribution and peak sizes recovered by 'unfolding'.

	10% normal noise			15% normal noise			10% uniform noise		
	RND†	$p7$	$p3$	RND	$p7$	$p3$	RND	$p7$	$p3$
Avg%	99.6	101.0	99.1	101.8	100.2	99.9	101.5	100.3	101.1
STD%	10.2	9.5	11.3	13.4	13.1	17.5	9.6	9.3	11.0
Max%	28	22	29	37	36	41	15	26	33
Min%	−18	−19	−25	−29	−31	−43	−18	−19	−32

† RND is a sample of the random noise generated, $p7$ and $p3$ indicate the peak heights of ν_3 and ν_1 recovered, here scaled up to give a common theoretical average (Avg) of 100. The number of repetitions is 120. STD = standard deviations in per cent of average, Max% and Min% are similarly defined maximum and minimum deviations from the average.

Table A2. Statistics of a 4-peak simulation[a].

Peaks	Elastic	$p7$	$p3$	$p1$	Sum($p3 + p1$)
Position (meV)	0	112.5	128	122.2	∼125.1
Avg%	99.5	99.7	97.0	111.3	101.3
STD%	3.24	9.4	25.0	91.3	15.75
Max%	9.12	28.9	59.3	247	44.4
Min%	−8.6	−25.1	−66.2	−267	−50.4

[a] Recovered peak sizes for 10% normal noise when the simulated data set includes the 1.5% peak marked as $p1$. $N = 150$. Symbols as in table A1. Sum($p3 + p1$) is the statistics of the simple sum of the $p3$ and $p1$ heights.

to those of the original data but errors of the smaller peak are somewhat larger (1.3 times).

A.2. On the inclusion of $2\nu_4$ in the unfolding process

So far we have assumed that only ν_1 and ν_3 had to be considered in the region of interest up to about 0.14 eV from the elastic peak while actually several modes and combination frequencies are present: ν_4 (0.0601 eV), ν_2 (0.0802), ν_3 (0.1125), $2\nu_4$ (0.1222), ν_1 (0.1280), $\nu_4 + \nu_3$ (0.1413). The first two are small in size (about 0.5% of the elastic peak) and difficult to separate from its tail; they are included in the actual unfoldings only to cover the valley there, so that ν_3 does not have to fulfil this function. The combination peak $\nu_4 + \nu_3$ with approximate size 0.6% is 0.5 apparatus-resolutions away from ν_1 and can be as easily distinguished as previously ν_1 and ν_3. It should not influence the analysis of ν_1/ν_3. For $2\nu_4$ two cases must be distinguished: (a) $2\nu_4$ included in the simulated data and in the analysis, and (b) $2\nu_4$ included in the analysis but not in the simulated data set. The results for case (a) with an arbitrarily assumed peak size of 1.5% for $2\nu_4$ are shown in table A2. The elastic peak involves no ratio and thus shows a considerable error reduction. Peaks 3.5% and 1.5% interfere with one another but do not modify the analysis of the 7% peak. Their separation amounts to $\frac{1}{6}$–$\frac{1}{7}$ of the instrumental FWHM, and they should then be combined into a single peak as the last column of the table indicates. This column is the simple sum of the 3.5% and 1.5% peaks recovered (i.e. without combining them into a single peak at 125.1 eV).

In case (b) when the 1.5% peak is excluded from the simulated data set but included in the analysis, the story changes considerably. Out of 100 trials, 40 resulted in negative peak sizes for $2\nu_4$, 25 produced an unacceptable shape of the ν_1/ν_3 compound peak (mostly wrongly centred), and 25 would have been accepted as good fits, half of these as very good

fits—that is, if we were doing only one single unfolding at one single scattering angle. While the inclusion of $2\nu_4$ may be successful at one scattering angle, it was impossible to achieve a consistent behaviour over the loss spectra at all scattering angles. Negative coefficients arise in about 90% when the position of $2\nu_4$ is shifted towards ν_1 by 2–3 meV.

The possibility of negative peak sizes constitutes at the same time the strength and weakness of *linear* least square fitting. As a check, we are now preparing a nonlinear program that uses the squares of the peak sizes as fitting parameters, but expect to find many local minima.

References

Abramowitz M and Stegun I A 1972 *Handbook of Mathematical Functions* (New York: Dover) ch 26–8

Alle T D, Gulley R J, Buckman S J and Brunger M J 1992 *J. Phys. B: At. Mol. Opt. Phys.* **25** 1533–42

Andrick D and Read F H 1971 *J. Phys. B: At. Mol. Phys.* **4** 389–96

Baumgärtel H, Jochims H W, Rühl E, Bock H, Dammel R, Minkwitz J and Nass R 1989 *Inorg. Chem.* **28** 943–9

Bawagan A O and Brion C E 1987 *Chem. Phys. Lett.* **137** 573–7

——1988 *Chem. Phys.* **123** 51–63

Ben Arfa M and Tronc M 1985 *J. Phys. B: At. Mol. Phys.* **18** L629–32

——1988 *J. Chim. Phys.* **85** 889–97

Blanks K A and Becker K 1987 *J. Phys. B: At. Mol. Phys.* **20** 6157–63

Blanks K A, Tabor A E and Becker K 1987 *J. Chem. Phys.* **86** 4871–5

——1989 *Int. Conf. on Physics of Electronic and Atomic Collisions (Brighton)* p 347

Boesten L 1988 *Rev. Sci. Instrum.* **59** 233–7

Boesten L and Tanaka H 1991 *J. Phys. B: At. Mol. Opt. Phys.* **24** 821–32

——1992 *At. Data Nucl. Data Tables* **52** 25–42

Bransden B H 1970 *Atomic Collision Theory* (New York: Benjamin) ch 1

Brinkmann R T and Trajmar S 1981 *Rev. Sci. Instrum.* **14** 245–54

Buckman S J, Gulley R J and Brunger M J 1994 *Electron Collisions with Molecules, Clusters and Surfaces* ed H Ehrhardt and L A Morgan (New York: Plenum) pp 87–104

Chantry P J 1978 Electron attachment plot as found in Ushinoda S, Kajita S and Kondo Y 1990 *J. Phys. D: Appl. Phys.* **23** 47–52

Chen D and Gallup A 1990 *J. Chem. Phys.* **93** 8893–901

Dillon M A, Boesten L, Tanaka H, Kimura M and Sato H 1993 *J. Phys. B: At. Mol. Opt. Phys.* **26** 3147–58

Donnelly V M, Flamm W C, Dautremont-Smith W C and Werder D J 1984 *J. Appl. Phys.* **55** 242–52

Fluck and Heumann 1991 Table produced by VCH-Verlagsgesellschaft (Weinheim, Germany)

Frisch *et al* 1992 *GAUSSIAN 92 Revision C* (Pittsburgh, PA: Gaussian)

Gianturco F A 1991 *J. Phys. B: At. Mol. Opt. Phys.* **24** 4627–48

Gianturco F A, Lucchese R and Sanna N 1994 *J. Chem. Phys.* **100** 6464–71

Gianturco F A and Thompson D G 1980 *J. Phys. B: At. Mol. Phys.* **13** 613–25, 622f

Gillespie R J and Robinson E A 1992 *Inorg. Chem.* **31** 1960–3

Gladney H M, Dowden B F, and Swalen J D 1969 *J. Comput. Phys.* **2** 883–8

Greenberg K E and Verdeyen J T 1985 *J. Appl. Phys.* **57** 1596–601

Gulley R J, Brunger M J and Buckman S J 1992 *J. Phys. B: At. Mol. Opt. Phys.* **25** 2433–40

Hall R I and Read F H 1984 *Electron–Molecule Collisions* ed I Shimamura and K Takayanagi (New York: Plenum) pp 351–425

Hargis P J and Greenberg K E 1990 *J. Appl. Phys.* **67** 2767–73

Harland P W and Franklin J L 1974 *J. Chem. Phys.* **61** 1621–36

Herzberg G 1945 *Molecular Spectra and Molecular Structure* vol II (New York: Van Nostrand)

Huo W M 1995 Private communication (October)

Itikawa Y and Nishimura T 1995 *Ann. Conf. Jap. Phys. Soc. (Yokohama)* **50** 30p YR8

Jauhiuainen J, Kivimäki A, Aksela S, Sairanen O-P and Aksela H 1995 *J. Phys. B: At. Mol. Opt. Phys.* **28** 4091–100

Jabbour Z J, Blanks K A, Martus K E and Becker K 1988 *J. Chem. Phys.* **88** 4252–6

Jäger S, von Jouanne J, Keller-Rudek H, Koshel D, Kuhn P, Merlet P, Rupecht S, Vanacek H and Wagner J 1986 *Gmelin Handbook of Inorganic Chemistry* 8th edn vol F suppl 4 (Berlin: Springer) section 4.1.4.6

Johnstone W M and Newell W R 1991 *J. Phys. B: At. Mol. Opt. Phys.* **24** 3633–42

——1993 *J. Phys. B: At. Mol. Opt. Phys.* **26** 129–38

Johnstone W M, Akther P, and Newell W R 1995 *J. Phys. B: At. Mol. Opt. Phys.* **28** 743–53
Koonin S E 1986 *Computational Physics* (Menlo Park CA: Benjamin/Cummings) ch 4 (you have to run the programs to see the shape of the DCS)
Korn G A and Korn T M 1968 *Mathematical Handbook for Scientists and Engineers* (New York: McGraw-Hill) table 18.8-8
Kuyatt C E and Simpson J A 1967 *Rev. Sci. Instrum.* **38** 103–11
Lakdawala V K and Moruzzi J L 1980 *J. Phys. D: Appl. Phys.* **13** 377–85
Landau L D and Lifshitz E M 1965 *Quantum Mechanics* (Oxford: Pergamon)
Merlet P *et al* (ed) 1986 *Gmelin Handbook of Inorganic Chemistry* 8th edn, vol F (Berlin: Springer) supplement 4, section 4.1.4.6
Nickel J C, Zetner P W, Shen G and Trajmar S 1989 *Rev. Sci. Instrum.* **22** 730–8
Nihon-Kagakkai (= Jap. Chem. Soc.) (ed) 1984 Kagaku Binran vols I, II (Tokyo: Maruzen) (in Japanese)
Okamoto Y, Onda K and Itikawa Y 1993 *J. Phys. B: At. Mol. Opt. Phys.* **26** 745–58
O'Keeffe M 1986 *J. Am. Chem. Soc.* **108** 4341–3
Onda K 1994 Private communication (November)
Onda K and Truhlar G 1980 *J. Chem. Phys.* **73** 2688–95
Pitha J and Jones N 1966 *Can. J. Chem.* **44** 3031–50
Press W H, Flannery B P, Teukolsky S A, and Vetterling W T 1988 *Numerical Recipes in C* (Cambridge: Cambridge University Press) pp 204ff
Pritchard H P, Lima M A P and McKoy V 1989 *Phys. Rev.* A **39** 2392–6
Randell J, Field D, Lunt S L, Mrotzek G, and Ziesel J P 1992 *J. Phys. B: At. Mol. Opt. Phys.* **25** 2899–909
Register D F, Trajmar S and Srivastava S K 1980 *Phys. Rev.* A **21** 1134–51
Rescigno T N 1995a *Phys. Rev.* A **52** 329–33, data used in figure 3 from a private communication
——1995b *XIX ICPEAC (Whistler, Canada July 1995)* p 22
Roberts S M, Wilkinson D H, and Walker L R 1970 *Anal. Chem.* **42** 886–93
Rogers S A, Miller P J, Leone S R and Brehm B 1990 *Chem. Phys. Lett.* **166** 137–40
Roque M B, Siegel R B, Martus K E, Tamovsky V and Becker K 1991 *J. Chem. Phys.* **94** 341–50
Schmid E W, Spitz G and Lösch W 1988 *Theoretical Physics on the Personal Computer* (Berlin: Springer) ch 19 (you have to run the programs to see the shape of the DCS)
Shimanouchi T 1972 *Tables of Molecular Vibrational Frequencies I (NSRDS-NBS 39)* (Natl Bur. Stand. US)
Sides G D and Tiernan T O 1977 *J. Chem. Phys.* **67** 2382–4
Sueoka O, Mori S and Katayama Y 1987 *J. Phys. B: At. Mol. Phys.* **20** 3237–46
Szmytkowski C, Maciąg K, Karwasz G and Filipović D 1989 *J. Phys. B: At. Mol. Opt. Phys.* **22** 525–30
Takagi T, Boesten L, Tanaka H and Dillon M A 1994 *J. Phys. B: At. Mol. Opt. Phys.* **27** 5389–404
Tanaka H, Boesten L, Sato H, Kimura M, Dillon M A and Spence D 1990 *J. Phys. B: At. Mol. Opt. Phys.* **23** 577–88
Tanaka H, Kubo M, Onodera N and Suzuki A 1983 *J. Phys. B: At. Mol. Phys.* **16** 2861-9
Tarnovsky V, Levin A, Becker K, Basner R and Schmidt M 1994 *J. Mass. Spectrom. Ion Process.* **133** 175–85
Thomas R J, Bradley J, DeLeeuw J, Vacek G, Crawford T D, Yamaguchi Y and Schaefer H F III 1993 *J. Chem. Phys.* **99** 403–16
Thompson D G 1966 *Proc. R. Soc.* A **294** 160–74
Thomsen J W, Andersen N, Dowek D, Houver J C, Larsson M U, Lauritsen J H V, Müller U, Pedersen J O P, Salgado J and Svensson A S 1995 *J. Phys. B: At. Mol. Opt. Phys.* **28** L93–9
Thynne J C J 1969 *J. Phys. Chem.* **73** 1586–8
Trainor D W and Jacob J H 1979 *J. Appl. Phys.* **35** 920–2
Trajmar S and Register D F 1984 *Electron–Molecule Collisions* ed I Shimamura and K Takayanagi (New York: Plenum) pp 427–93
Weast R C (ed) 1987 *Handbook of Chemistry and Physics* (Boca Raton, FL: Chemical Rubber Company) E-64
Winstead C, Sun Q and McKoy V 1993 *J. Chem. Phys.* **98** 1105–9
Wong S F and Dubé L 1978 *Phys. Rev.* A **17** 570–6
Wong S and Schulz G J 1975 *Phys. Rev. Lett.* **35** 1429–30